Journal of Solid State Chemistry **161,** 17–22 (2001)
doi:10.1006/jssc.2001.9261, available online at http://www.idealibrary.com on IDEAL®

Unique Periodic Modulations in the Infinite $[Te_x]^{n-}$ Chains of $RbUSb_{0.33}Te_6$

Kyoung-Shin Choi and Mercouri G. Kanatzidis[1]

Department of Chemistry, Michigan State University, East Lansing, Michigan 48824-1322

Received May 16, 2001; accepted May 25, 2001; published online August 31, 2001

The new phase $RbUSb_{0.33}Te_6$ is described. The structure of $RbUSb_{0.33}Te_6$ is acentric and trigonal (space group $P3$) with infinite $[UTe_6]^{2-}$ columns running along the c axis. The structure has straight $[UTe_6]^{6-}$ columns in which the U atoms adopt distorted tri-capped trigonal prisms. The central axis in the $[UTe_6]^{2-}$ columns is defined by a row of U atoms 4.064 (1) Å apart, i.e., a metal "wire" seethed with what appear to be three infinite zig-zag Te chains. The crystals, however, exhibit a superstructure that results in a rhombohedral space group which is 9 times larger ($a_{super} = \sqrt{3}a_{sub}$, $b_{super} = \sqrt{3}b_{sub}$, $c_{super} = 3c_{sub}$) than that of the ideal $P3$ structure. The superstructure is caused by a periodic modulation of Te–Te distances in the zig-zag chains. The almost equal Te–Te distances in the infinite chains are in fact *dimers*, *trimers*, and *pentamers*. The material is a narrow gap semiconductor with a room temperature electrical conductivity of ~ 40 S/cm. © 2001 Academic Press

Key Words: **tellurium chains; polytelluride; superstructure; Peierls distortion; actinides.**

The distinguishing feature of Te, vis a vis its lighter congeners (i.e., S and Se), is its propensity to form Te ⋯ Te interactions beyond the normal catenation property of forming covalent Te–Te bonds (at < 2.8 Å) (1). This occurs through long-range lone-pair/lone-pair interactions to give extended even infinite aggregates. The lone-pair interactions are thought to be relativistic in nature and are defined by short Te ⋯ Te distances in the 2.8 to 3.5 Å range (2). These distances are too short to be considered van der Waals type and too long to be viewed as single bonds, yet they allow electronic delocalization between the Te atoms. The vast majority of compounds with Te ⋯ Te interactions contain *square nets* as for example $LnTe_3$, $LnTe_3$ (3), $KBa_2Ag_3Te_6$ (4), UTe_3 (5), $CsCe_3Te_8$ (6), $KCuCeTe_4$ (7), and Cs_3Te_{22} (8). However, other unusual motifs such as infinite networks are encountered in $NaTe_3$ (9), $CsTe_4$ (10), Cs_4Te_{28} (11), $RbTe_5$ (12), $RbTe_6$ (13), and $(Et_4N)_2Te_{12}$ (14). The square nets are unstable and present elaborate structural distortions brought about by the aforementioned long Te ⋯ Te interactions. Interest in these polytelluride compounds stems from the need to understand these distortions and their causes since they invariably affect the observed physical properties. Such phenomena, common in two-dimensional nets (15, 16), are not generally observed in one-dimensional Te chains.

Here we describe the novel compound $RbUSb_{0.33}Te_6$ that exhibits Te ⋯ Te interactions resulting in what appear to be infinite zig-zag chains.

The structure of $RbUSb_{0.33}Te_6$ (17a) is acentric and trigonal with infinite $[UTe_6]^{2-}$ columns running along the c axis (Fig. 1A). There exist two crystallographically unique U atoms in the $[UTe_6]^{6-}$ columns and both U1 and U2 adopt distorted tri-capped trigonal prisms (see Fig. 1B). The $[UTe_6]^{2-}$ columns form as the trigonal prisms of U1 and U2 share triangular faces (Fig. 1C). The distortion in the prisms is mainly due to the position of the capping Te atoms: instead of being exactly in the middle of the rectangular face they lie closer to the apex Te atoms to form Te ⋯ Te interactions (3.0–3.3 Å). This causes the local environment to bear resemblance to a pinwheel (see Fig. 1C). Since the distortion occurs in opposite directions for U1 and U2, the former can be considered a right-handed pinwheel and the latter a left-handed pinwheel, thus being chiral images to each other (the two would rotate in the wind in opposing directions!).

The central axis in the $[UTe_6]^{2-}$ columns is defined by a row of U atoms 4.064(1) Å apart, i.e., a metal "wire" seethed with three infinite zig-zag Te chains. Each chain has Te atoms with alternating bent (Te1 and Te3) and linear coordination (Te2 and Te4) (Fig. 1D). The average Te ⋯ Te distance of 3.06 Å is longer than normal Te–Te single bonds, found in elemental Te (2.83 Å), or in the isolated ditelluride bonds, $(Te_2)^{2-}$ of Rb_2Te_2 (2.78 Å) (18). Based on the fundamental valence shell electron pair repulsion (VSEPR) theory, the oxidation state of the bent Te atoms can be assigned as Te^0 and the linear Te atoms as Te^{2-} (see Scheme 1). Therefore, the chains in $RbUSb_{0.33}Te_6$ can be viewed as reduced versions of those in elemental Te by replacing every

[1]To whom correspondence should be addressed. E-mail: kanatzid@cem.msu.edu.

0022-4596/01 $35.00

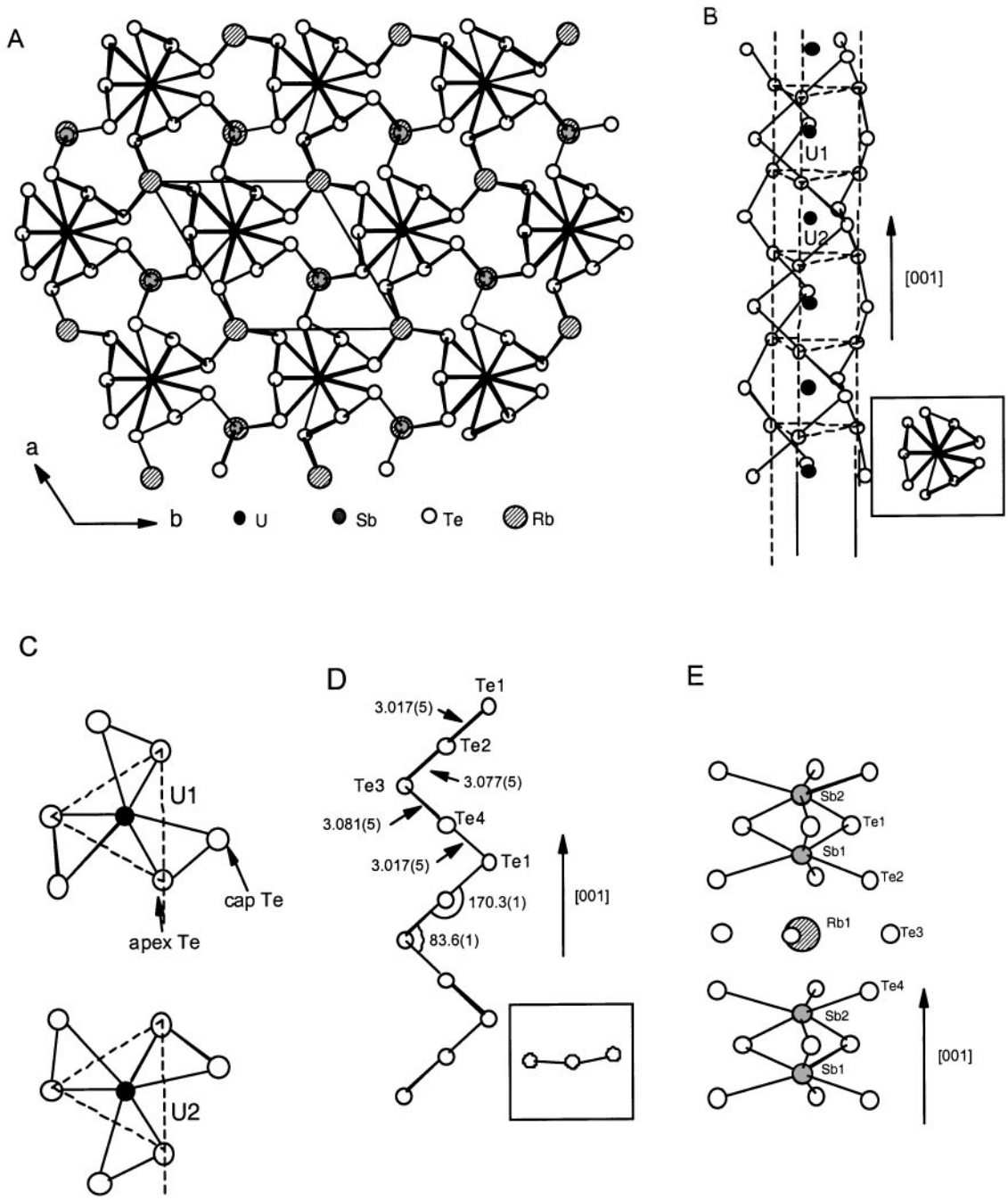

FIG. 1. (A) The structure of $RbUSb_{0.33}Te_6$ viewed down the *c* axis; (B) the one-dimensional UTe_6 column composed of tri-capped trigonal prisms sharing triangular faces. Projection of the column along the *c* axis is shown in box. The U–Te distances vary from 3.129(3) to 3.178(3) Å. (C) coordination environment of U(1) and U(2) atoms looking down the c-axis the pinwheel resemblance is clear; (D) the observed infinite zig-zag Te chain with bond distances (Å) and angles (°). Projection along the *c* axis is shown in the box; (E) arrangement of Sb and Rb atoms along the *c* axis.

other Te^0 atom with a linearly coordinated Te^{2-} atom. Alternatively, the chains can be perceived as a simple polymerization of Te^{-1} ions.

The Sb and Rb atoms occur in a sequence of –Sb(2)–Sb(1)–Rb(1)–, along the *c* axis and bridge the $[UTe_6]^{2-}$ columns (see Fig. 1E). All Sb atoms are stabilized in trigonal pyramidal sites, but they appear disordered with a Sb(1)–Sb(2) distance of 2.23(5) Å, which is too short to allow both Sb(1) and Sb(2) to be present at the same time (19). The sum of all Sb site occupancies, refined without any

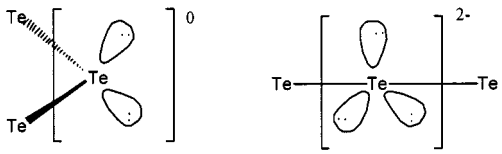

SCHEME 1.

constraint, adds up to 0.33 equiv., which is the exact value needed to balance the charge as $Rb^+U^{4+}(Sb^{3+})_{0.33}(Te_6)^{6-}$.

The structure of $RbUSb_{0.33}Te_6$ seems to be related to that of $CsUTe_6$ (20). The latter features double $[UTe_6]^-$ columns linked with ditelluride fragments. However, each column contains one infinite zig-zag Te chain very similar to what is observed in $RbUSb_{0.33}Te_6$.

A close inspection of the diffraction properties of $RbUSb_{0.33}Te_6$ in fact reveals weak superstructure reflections associated with a periodic modulation of the structure in real space (17b). Fortunately, we were able to measure enough satellite reflections to elucidate the important features of the structural modulation.

SUPERSTRUCTURE

The unit cell for the superstructure becomes rhombohedral and is nine times larger than that of the ideal structure which is indicated with dashed lines for comparison (see Fig. 2A). The superstructure is caused by a periodic modulation of Te–Te distances in the zig-zag chains. The almost equal Te–Te distances in the infinite chains now condense into *dimers*, *trimers*, and *pentamers* (Fig. 2B). All three chains around each uranium column present the same modulation pattern. The Te–Te distances within these oligomers are shorter (<3.07 Å) than the Te–Te distances between them (>3.13 Å). However, the distances in these oligomers are still somewhat longer than normal Te–Te bonds suggesting substantial interoligomer interactions. The charge of these fragments can be formally assigned as $(Te_2)^{2-}$, $(Te_3)^{2-}$, and $(Te_5)^{6-}$ based on simple VSEPR theory.

The modulation pattern in the Te chains of $RbUSb_{0.33}Te_6$ is unique, as we are not aware of similar 1D Te distortions in the literature. Undistorted the chains have a negative charge $(Te_6)^{6-}$, which would have to be delocalized along the entire chain. To lower the energy of such a system the chain distorts by modulating the Te–Te distances. Such distortion can be easily understood as a rendition of the one-dimensional Peierls distortion, which results in a lowering of the filled orbital (HOMO) energy levels and opening a HOMO-LUMO gap (21). No such modulation in the zig-zag Te chains was reported in $CsUTe_6$ (20).

The refinement of the superstructure also provides a better picture of the cationic arrangement in the channels as well. We observe two types of channels with different arrangement of Rb and Sb atoms. In channel type-I, the Sb atoms are ordered appearing as two independent Sb atoms, each with occupancy of 50% (see Fig. 3A). The Rb(1) and Rb(2) positions are resolved into two unique sites. The positional disorder of the Rb sites is forced by the partial occupancy of the Sb atoms, as the Rb atom attempts to adjust its position depending on whether Sb is present or not. Between Rb(2) and Rb(1) along the channel, there exists a Sb "vacancy" compared with the Sb array in the substructure. Therefore, the average Sb occupancy in channel I is 33% [$\frac{1}{3}${50% (Sb1) + 48% (Sb2) + 0% (for the vacancy)}].

In channel II, there exist three independent Sb atoms, all of which are disordered over two sites. The three independent Rb atoms between these disordered Sb sites are also disordered due to the partial occupancy in the disordered Sb sites (see Fig. 3B). For example for 66% of the time when both Sb(3) and Sb(4) are absent, the Rb(4) position is occupied. For 18% of time when Sb(3) is present, Rb(4) moves down to the position of Rb (4″) to achieve an optimum Rb–Sb distance of 3.88(7) Å. For 15% of the time when Sb(4) is present, Rb(4) is pushed up to the Rb(4′) position and the distance between Sb(4) and Rb(4′) becomes 3.94(7) Å. The average occupancy of Sb in the channel II is again ~33% [18% (Sb3) + 15% (Sb4)] (22).

The presence of a HOMO-LUMO gap is supported the charge transport properties of $RbUSb_{0.33}Te_6$. The material is a narrow gap semiconductor. The electrical conductivity of single crystal samples at room temperature is only ~40 S/cm. This value is consistent with a semiconductor yet it is high enough to suggest substantial carrier delocalization along the structure. The conductivity increases with increasing temperature, indicating classical thermally activated, semiconducting behavior (see Fig. 3C) (23). The activation energy for charge transport is ~0.05 eV as calculated from the data of Fig. 3C. The thermopower is very large at room temperature with a Seebeck coefficient of $\sim +210\ \mu V/K$, and exhibits very weak temperature dependence (see Fig. 3D). The positive sign indicates that the material is a p-type semiconductor. The holes are most likely based on Te orbitals. The magnetic susceptibility follows Curie–Weiss behavior between 20 and 300 K with $\mu_{eff} = 3.04$, B.M. and $\theta = -6.3$ K. The magnetic moment suggests $5f^2$ electron configuration and U^{4+}.

The zig-zag Te chains in $RbUSb_{0.33}Te_6$ present a unique type of modulation in the Te–Te distances that causes a nine-fold superstructure ($a_{super} = \sqrt{3}a_{sub}$, $b_{super} = \sqrt{3}b_{sub}$, $c_{super} = 3c_{sub}$). The conformation of these chains is different from the more familiar helical chains found in elemental Te (24), $CuTeX$ (25), and $CuTe_2X$ (26) (X = Cl, Br, I) or the zig-zag chains of $ZrTe_5$ (27), or the straight chains in CuTe (28) As far as we know these systems do not present any type of modulation.

EXPERIMENTAL

$RbUSb_{0.33}Te_6$: The compound was synthesized from a mixture of 0.1194 g (0.4 mmol) Rb_2Te, 0.0952 g (0.4 mmol)

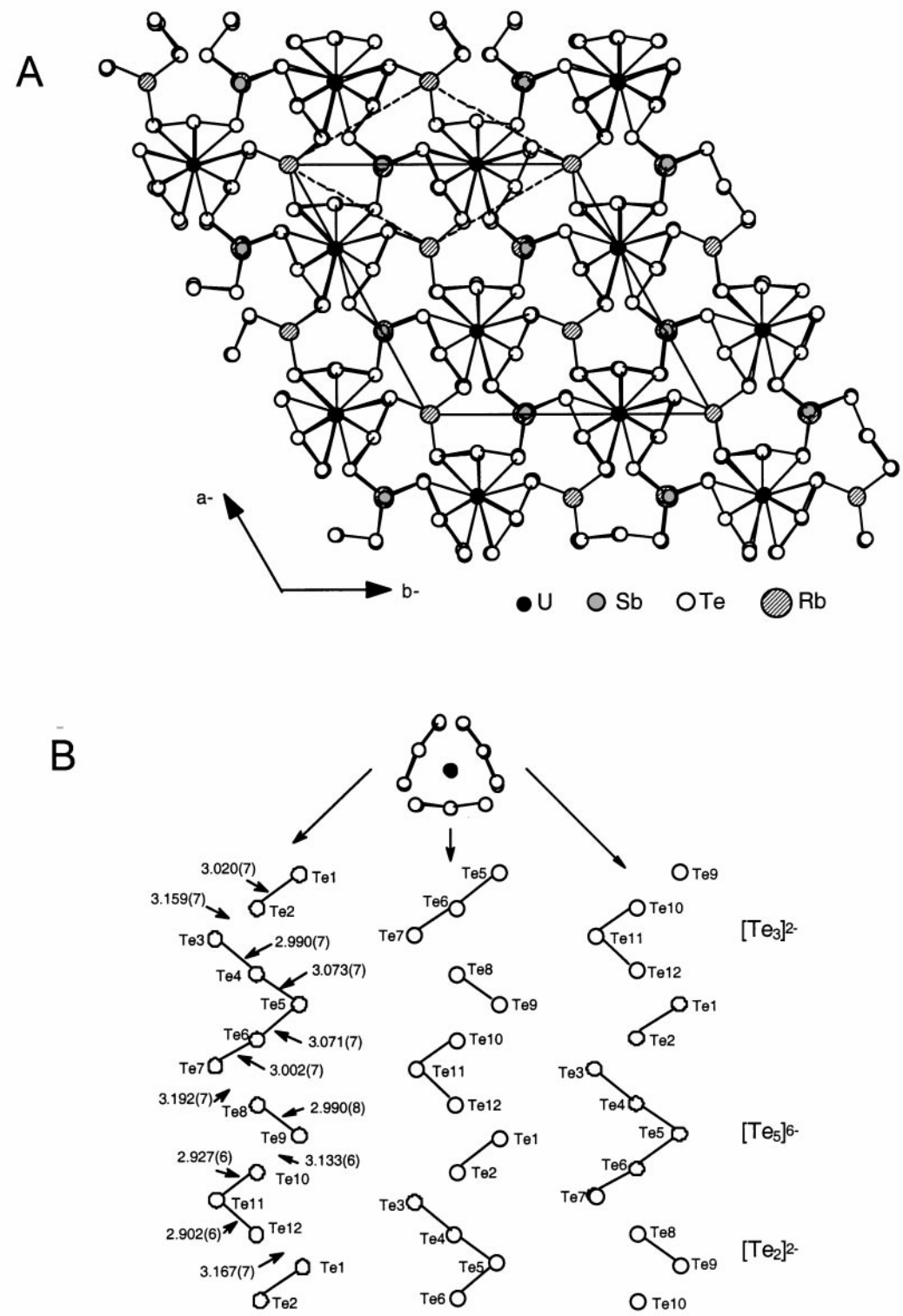

FIG. 2. (A) The superstructure of $RbUSb_{0.33}Te_6$ as viewed down the *c* axis. The unit cell of the substructure is shown in dashed lines for comparison; (B) the periodic modulations in the Te chains resulting in dimers, trimers, and pentamers.

U, 0.0244 g (0.2 mmol) Sb, and 0.2552 g (2.0 mmol) Te. The reagents were thoroughly mixed, sealed in an evacuated silica ampoule, and heated at 720°C for 5 days (cooling 2°C/h). Pure black needle-like crystals of $RbUSb_{0.33}Te_6$ were obtained after removing the flux with dimethylformamide and water (yield ~80% based on U). The crystals

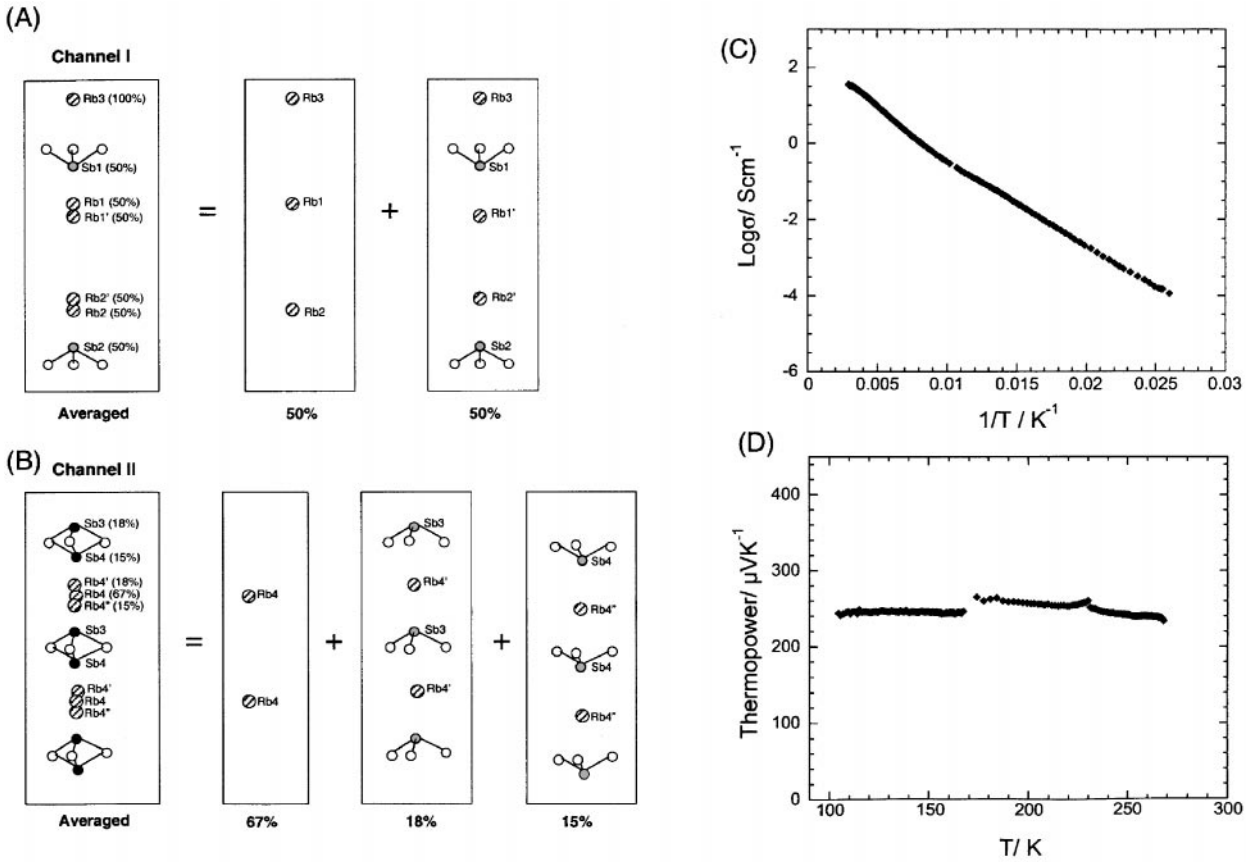

FIG. 3. The arrangements of Sb and Rb atoms along the *c* axis of the superstructure (A) channel type-I and (B) channel type-II. When Sb(1) is absent, Rb can be stabilized in its ideal Rb(1) site. When Sb(1) is present, the distance between Rb(1) and Sb(1) gets too close (2.66(2) Å) and Rb(1) must move 1.03(2) Å along *c* toward the Rb(1′) position to allow enough space for Sb(1). The distance between Rb(1′) and Sb(1) then becomes a reasonable 3.69(2) Å. The situation for Sb(2), Rb(2), and Rb(2′) is similar. Only the position of Rb(3), which is 5.2 Å away from both Sb(1) and Sb(2), is not affected by the presence of Sb atoms and is fully occupied in a single position without disorder. (C) $\log \sigma$ vs $1/T$ plot of the electrical conductivity for a crystal of $RbUSb_{0.33}Te_6$. The nearly linear dependence suggests a classical semiconductor with an activation energy gap. Part (D) represents the thermopower data for a single crystal of $RbUSb_{0.33}Te_6$.

are air and water stable and do not melt under 1000°C. The presence of Sb was verified with energy dispersive spectroscopic microprobe analysis. The Raman spectrum of $RbUSb_{0.33}Te_6$ shows shifts at 142, 125, 94, and 90 cm^{-1}, respectively.

ACKNOWLEDGMENT

We thank the National Science Foundation (DMR-9817287) for support.

REFERENCES

1. M. G. Kanatzidis, *Angew. Chemie, Int. Ed. Engl.* **34,** 2109–2111 (1995).
2. P. Pyykko, *Chem. Rev.* **97,** 597–636 (1997).
3. (a) W. Lin, H. Steinfink, and E. J. Weiss, *Inorg. Chem.* **4,** 877–881 (1965); (b) R. Wang, H. Steinfink, and W. F. Bradley, *Inorg. Chem.* **5,** 142–145 (1966); (c) T. H. Ramsey, H. Steinfink, and E. J. Weiss, *Inorg. Chem.* **4,** 1154–1157 (1965); (d) B. K. Norling and H. Steinfink, *Inorg. Chem.* **5,** 1488–1491 (1966).
4. X. Zhang, J. Li, B. Foran, S. Lee, H.-Y. Guo, T. Hogan, C. R. Kannewurf, and M. G. Kanatzidis, *J. Am. Chem. Soc.* **117,** 10,513–10,520 (1995).
5. (a) K. Stowe, *Z. Anorg. Allg. Chem.* **623,** 749–754 (1997); (b) K. Stowe, S. Tratzky, H. P. Beck, A. Jungmann, R. Claessen, R. Zimmermann, G. Meng, P. Steiner, and S. Hufner, *J. Alloy Compd.* **246,** 101–110 (1997); (c) K. Stowe, *Z. Anorg. Allg. Chem.* **622,** 1423–1427 (1996); (d) H. Noel and J. C. Levet, *J. Solid State Chem.* **79,** 28–33 (1989).
6. R. Patschke, J. Heising, J. Schindler, C. R. Kannewurf, and M. G. Kanatzidis, *J. Solid State Chem.* **135,** 111–115 (1998).
7. R. Patschke, J. Heising, P. Brazis, C. R. Kannewurf, and M. G. Kanatzidis, *Chem. Mater.* **10,** 695–697 (1998).
8. W. S. Sheldrick and M. Wachhold, *Angew. Chem. Int. Ed. Engl.* **34,** 440 (1995).
9. P. Böttcher and R. Keller, *J. Less-Common Met.* **109,** 311 (1985).
10. P. Böttcher and U. Kretschmann, *Z. Anorg. Allg. Chem.* **523,** 145–152 (1985).
11. W. S. Sheldrick and M. Wachhold, *Chem. Commun.* **5,** 607–608 (1996).
12. P. Böttcher and U. Kretschmann, *J. Less-Common Met.* **95,** 81–91 (1983).
13. W. S. Sheldrick and B. Schaaf, *Z. Naturforsch. B* **49,** 993–996 (1994).

14. C. J. Warren, R. C. Haushalter, and A. B. Bocarsly, *J. Alloys Compd.* **233**(1–2), 23–29 (1996).
15. (a) B. Foran, S. Lee, and M. C. Aronson, *Chem. Mater.* **5,** 974–978 (1993); (b) S. Lee and B. Foran, *J. Am. Chem. Soc.* **116,** 154–161 (1994); (c) K. Stöwe, *J. Solid State Chem.* **149,** 155–166 (2000); (d) O. Gourdon, J. A. Hanko, F. Boucher, V. Petricek, M.-H. Whangbo, M. G. Kanatzidis, and M. Evain, *Inorg. Chem.* **39,** 1398–1409 (2000).
16. (a) E. DiMasi, M. C. Aronson, J. F. Mansfield, B. Foran, and S. Lee, *Phys. Rev. B.* **55**(20), 14,516–14,525 (1995); (b) G. H. Gweon, J. D. Denlinger, J. A. Clack, J. W. Allen, C. G. Olson, E. DiMasi, M. C. Aronson, B. Foran, and S. Lee, *Phys. Rev. Lett.* **81,** 886–889 (1998); (c) E. DiMasi, B. Foran, M. C. Aronson, and S. Lee, *Chem. Mater.* **6,** 1867–1874 (1999).
17. (a) Substructure: Crystal dimensions $0.18 \times 0.05 \times 0.03\ \mathrm{mm}^3$, space group $P3$, $a = 9.0925$ (14) Å, $c = 8.129$ (2) Å, $V = 582.0$ (2) Å^3, $Z = 2$, $D_{\mathrm{calc}} = 6.454\ \mathrm{g/cm}^3$, μ (Mo$K\alpha$) $= 335.30\ \mathrm{cm}^{-1}$, total data = 5473, unique data = 1780 ($R_{\mathrm{int}} = 0.047$); No. of variables = 60, $R1/\mathrm{w}R2$ ($I > 2\sigma$) = 0.068/0.156, GOF on $F^2 = 1.19$, BASF = 0.14 (2). (b) During data collection, we observed very weak reflections that could not be a indexed based on the initial cell (subcell) parameters. These gave rise to a supercell ($a_{\mathrm{super}} = \sqrt{3}a_{\mathrm{sub}}$, $b_{\mathrm{super}} = \sqrt{3}b_{\mathrm{sub}}$, $c_{\mathrm{super}} = 3c_{\mathrm{sub}}$). Superstructure: space group $R3$, $a = 15.741$ (2) Å, $c = 24.382$ (4) Å, $V = 5231.9$ (4) Å^3, $Z = 18$, $D_{\mathrm{calc}} = 6.454\ \mathrm{g/cm}^3$, μ (Mo$K\alpha$) $= 335.67\ \mathrm{cm}^{-1}$, total data = 14.489, unique data = 4095 ($R_{\mathrm{int}} = 0.053$); No. of variables = 184, $R1/\mathrm{w}R2$ ($I > 2\sigma$) = 0.07/0.097, GOF on $F^2 = 1.151$, BASF = 0.14 (2). A Bruker SMART Platform CCD diffractometer using graphite monochromated Mo$K\alpha$ radiation ($\lambda = 0.71073$ Å) was used for data collection. Several different sets of frames, covering a random area of the reciprocal space, were collected using 0.3 steps in ω with a acquisition time of 70 s at room temperature. The SMART and SAINT software were used for data acquisition and extraction. Absorption correction was carried out with SADABS and the structure solution (direct methods) and refinement (full-matrix least squares on F^2) with SHELX97 (25). Further details of the crystal structure investigations may be obtained from the Fachinformationszentrum Karlsruhe, D-76344 Eggenstein-Leopoldshafen, Germany (fax: (+49) 7247-808-666; E-mail: crysdata@fiz-karlsruhe.de) on quoting numbers CSD-411660, and 411661.
18. P. Böttcher, J. Getzschmann, and R. Keller, *Z. Anorg. Allg. Chem.* **619,** 476–488 (1993).
19. All Sb atoms initially showed unusually high temperature factors warranting the occupancy of these sites to be refined. This refinement showed that all Sb sites are, on average, 16% occupied, i.e., ~16% of the time only Sb(1) is present, ~16% of time only Sb(2) is present, and 67% of the time both sites are empty. Sb(3) and Sb(4) behave similarly to Sb(1) and Sb(2) in the neighboring channel.
20. J. A. Cody and J. A. Ibers, *Inorg. Chem.* **34,** 3165–3172 (1995).
21. J. K. Burdett, "Chemical Bonding in Solids," Oxford Univ. Press, New York, 1995. pp. 48–52.
22. When Sb is absent, the Rb atoms (Rb(1) through Rb(4)) are 9-coordinate in tri-capped trigonal prismatic sites with Rb sitting on the same plane with three capping Te atoms. When Sb is present, Rb atoms sit between the trigonal face formed by three capping Te and one triangular face of the prism (top or bottom face of the prism depending on the direction from which Sb approaches). We cannot exclude the possibility of an even greater modulation that can lift the disorder of Sb and Rb.
23. We thank Prof. Carl Kannewurf for the electrical conductivity measurements.
24. C. Adenis, V. Langer, and O. Lindqvist, *Acta Crystallogr. Sect. C; Cryst. Struct. Commun.* **45,** 941–942 (1989).
25. (a) J. Fenner and H. Schulz, *Acta Crystallogr. Sect. B* **35,** 307–311 (1979); (b) P. M. Carkner and H. M. Haendler, *J. Solid State Chem.* **18,** 183–189 (1976); (c) W. Milius, *Z. Anorg. Allg. Chem.* **586,** 175–184 (1990).
26. (a) W. Milius, *Z. Naturforsch.* **44b,** 990–992 (1989); (b) J. Fenner, *Acta Crystallogr. Sect. B* **32,** 3084–3086 (1976).
27. H. Fjellvag and A. Kjekshus, *Solid State Commun.* **60,** 91–93 (1986).
28. S. Seong, T. A. Albright, X. Zhang, and M. G. Kanatzidis, *J. Am. Chem. Soc.* **116,** 7287–7294 (1994).